

Biologics-based technologies for highly efficient and targeted RNA delivery

Anastasiya Kostyusheva,^{1,14} Sergey Brezgin,^{1,2,14} Natalia Ponomareva,^{1,2} Anastasiia Frolova,^{1,2} Alexander Lunin,³ Ekaterina Bayurova,³ Andrey Tikhonov,¹ Olga Slatinskaya,⁴ Polina Demina,^{5,6} Artyom Kachanov,¹ Gulalek Babayeva,^{7,8} Irina Khan,^{7,8} Dmitry Khochenkov,^{7,9} Yulia Khochenkova,⁷ Darina Sokolova,^{2,7,8} Denis Silachev,^{10,11} Georgy Maksimov,⁴ Evgeny Khaydukov,^{5,6} Vadim S. Pokrovsky,^{7,8} Andrey A. Zamyatnin, Jr.,^{2,10,12} Alessandro Parodi,² Ilya Gordeychuk,³ Vladimir Chulanov,¹³ and Dmitry Kostyushev^{1,2,12}

¹Laboratory of Genetic Technologies, Martsinovsky Institute of Medical Parasitology, Tropical and Vector-Borne Diseases, First Moscow State Medical University (Sechenov University), Moscow 119435, Russia; ²Division of Biotechnology, Sirius University of Science and Technology, Sochi 354340, Russia; ³Chumakov Federal Scientific Center for Research and Development of Immunobiological Products, Russian Academy of Sciences (Polio Institute), Moscow 142782, Russia; ⁴Faculty of Biology, Lomonosov Moscow State University, Moscow 119234, Russia; ⁵Moscow Pedagogical State University, Moscow 119435, Russia; ⁶Shemyakin-Ovchinnikov Institute of Bioorganic Chemistry of the Russian Academy of Sciences, Moscow 117997, Russia; ⁷Blokhin National Medical Research Center of Oncology, Moscow 115522, Russia; ⁸RUDN University, Moscow 117198, Russia; ⁹Togliatti State University, Togliatti 445020, Russia; ¹⁰A.N. Belozersky Institute of Physico-Chemical Biology, Lomonosov Moscow State University, Moscow 119234, Russia; ¹¹V.I. Kulakov National Medical Research Center of Obstetrics, Gynecology and Perinatology, Moscow 117198, Russia; ¹²Faculty of Bioengineering and Bioinformatics, Lomonosov Moscow State University, Moscow 119192, Russia; ¹³Department of Infectious Diseases, First Moscow State Medical University (Sechenov University), Moscow 119435, Russia

The demand for RNA-based therapeutics is increasing globally. However, their use is hampered by the lack of safe and effective delivery vehicles. Here, we developed technologies for highly efficient delivery of RNA cargo into programmable extracellular vesicle-mimetic nanovesicles (EMNVs) by fabricating hybrid EMNV-liposomes (Hybs). Tissue targeting is endowed by highly efficient genetic platforms based on truncated CD63 (Δ CD63) or PTGFRN proteins. For the first time we reveal their efficiency in functionalizing EMNVs, resulting in >10-fold enhancement of nanoparticle internalization *in vitro* and >2-fold *in vivo*. RNA delivery using Hybs demonstrated efficiency of >85% in human and mouse cell lines. Comparative analysis of EMNVs and Hyb lysosome colocalization and stability suggested that Hybs enter the lysosomal compartment and escape over time, whereas EMNVs primarily avoid it. Finally, we used these technologies to generate liver-targeting Hybs loaded with therapeutic small interfering RNA and demonstrated the robust efficiency of this system *in vitro* and *in vivo*. These technologies can be adapted for manufacturing a wide range of next-generation vehicles for highly efficient, safe delivery of RNA into desired organs and tissues for therapeutic and prophylactic applications.

INTRODUCTION

Biological nanoparticles (NPs) are nanosized vesicles produced from virtually any human cells and possessing unique properties for drug-delivery applications, including safety, biocompatibility, ability to effectively cross biological barriers, and programming capacity (e.g., capacity for modification of their targeting properties and payloads

using different genetic and chemical methods).¹ Biological NPs are a large group of nanovesicles naturally produced by cells (exosomes, apoptotic bodies, microvesicles, and other extracellular vesicles [EVs]) or fabricated from cells. Cell-produced NPs include different biomimetics,^{2,3} nanoghosts,⁴ and extracellular vesicle-mimetic nanovesicles (EMNVs).^{5,6} EMNVs are produced from cells by applying pressure to cell pellets, extruding them through a set of differently sized filters. Major advantages of fabricated biological NPs and, in particular, EMNVs, compared to secreted NPs, are their extremely high production yields and homogeneity.⁷

In the past decade, the field of RNA therapeutics and vaccines has made a leap as dozens of therapies based on RNA-interference technologies (small interfering RNA [siRNA], short hairpin RNA [shRNA], microRNA [miRNA], and adenosine deaminase acting on RNA [ADAR] oligonucleotides) and mRNA vaccines have moved into the clinic.⁸ More recent RNA therapies based on CRISPR-Cas nucleases, base editors, and epigenetic modifiers are being developed for treating a wide range of hereditary and infectious diseases and cancers.^{9,10} Currently, the most investigated nanoplatforms for delivering RNA payloads *in vivo* include lipid-based NPs (lipid NPs,

Received 5 May 2024; accepted 4 November 2024;
<https://doi.org/10.1016/j.ymthe.2024.11.004>

¹⁴These authors contributed equally

Correspondence: Dmitry Kostyushev, Laboratory of Genetic Technologies, Martsinovsky Institute of Medical Parasitology, Tropical and Vector-Borne Diseases, First Moscow State Medical University (Sechenov University), Moscow 119435, Russia

E-mail: dkostushev@gmail.com

micelles, and liposomes) and polymers and polymer-based NPs (e.g., polylactic-co-glycolic acid, polyethyleneimine, poly-L-lysine).¹¹ Most studies demonstrate the ability of these technologies to deliver payloads into the liver and some efficacy in targeting the spleen, lungs, bone marrow, and pulmonary and cardiovascular endothelium.¹¹ Major drawbacks of these delivery platforms include toxicity, lack of efficient and cost-effective tissue/organ targeting, and accelerated clearance, especially after repeated administrations.¹¹ In this scenario, developing novel nanosystems for targeted and safe RNA delivery is urgently needed.

Biological NPs can be easily functionalized using genetic technologies based on the fusion of constitutive proteins of NPs (e.g., Lamp2B, CD63, lactadherin C1C2, GPI anchor) with targeting moieties.¹² These technologies were mostly developed for programming the surface of exosomes and other EVs. Recently, two novel, highly efficient peptide display technologies were introduced, namely truncated forms of CD63 (Δ CD63)¹³ and PTGFRN.¹⁴ However, their utility for biological NPs other than EVs is not known.

The idea of fusing exosomes with liposomes to take advantage of both NPs was first described by Nakase and Futaki¹⁵ to increase cellular uptake. Another milestone was the study by Piffoux et al., who tackled the problem of RNA loading by fusing EVs with liposomes to enrich EVs with virtually any hydrophilic or hydrophobic payloads.¹⁶ The key issue of these technologies is that fusion of two NPs increases their size over 200 nm, impairing their *in vivo* delivery properties, and their efficiency has not been studied previously.

In this study, we developed and utilized a series of robust technologies for safe, targeted, and highly efficient RNA delivery *in vivo*. The technology described is based on the fusion of EMNVs derived from human cells and functionalized with a specific targeting peptide using genetically encodable fusion proteins and RNA-loaded liposomes. The process includes an extrusion step to facilitate the fusion of EMNVs with liposomes, resulting in hybrid NPs with >2-fold improvement compared to previous methods and ensuring that the size of the resulting particles remains within an optimal range. This process confers targeting properties to the NPs through the incorporation of the targeting peptide and enables efficient loading of therapeutic or prophylactic RNA into the NPs. Compared to previous approaches, this technology offers several advantages: (1) it is more efficient than previously proposed incubation with liposomes; (2) it is scalable, with significantly higher yields of EMNVs and hybrid NPs compared to traditional EV production methods; (3) it can accommodate tunable amounts of unmodified or modified RNA molecules, expanding the range of RNA delivery options beyond conventional methods (e.g., chemically stabilized RNA, DNA-RNA hybrids); (4) it demonstrates the effectiveness of EV surface modification techniques for EMNVs and its preservation in produced hybrid NPs, and reveals the highest efficiency of PTGFRN genetic platform for peptide surface display; and (5) it generates NPs with optimal sizes for *in vivo* delivery. These technologies are adaptable for various biological NPs and biomimetic sys-

tems and can be utilized for organ- and tissue-specific RNA delivery.

RESULTS

Generation of biological and hybrid nanoparticles loaded with siRNA

First, we produced two types of carriers, EMNVs and hybrid EMNVs (Hybs) fused with commercial self-assembly liposomes (Lipofectamine 3000), using an extrusion process, as shown in Figure 1A. Cryogenic transmission electron microscopy (cryo-TEM) analysis demonstrated that EMNVs were spherical with clear margins, whereas the electron density of Hybs was heterogeneous, indicating uneven distribution of proteins and lipids (Figure 1B). Western blot analysis showed that both the formulations contained all major biomarkers of EVs as defined by MISEV2023 guidelines¹⁷ (Figure 1C). Next, we investigated the feasibility of synthesizing Hyb particles of ~100 nm (considered the optimal size range for *in vivo* delivery¹⁸). Lipofectamine 3000 reagents were first mixed with RNA to form liposomes. We then measured mean size and size distribution of EMNVs, liposomes, Hybs fused with liposomes, and extruded Hybs. These measurements demonstrated that liposomes were highly heterogeneous in size with a mean diameter of ~181 nm, whereas EMNVs had a mean size of ~88 nm (Figure 1D). Surprisingly, fusion of EMNVs with liposomes only slightly increased the size of Hybs, which was reduced after extrusion (Figure S1). Regardless of the selected amounts of liposomes, Hybs exhibited consistent size with a mean diameter ranging from approximately ~133 nm~139 nm (Figure 1D) and a uniform distribution (Figure 1E). Lipofectamine 3000, composed of cationic lipids, is known to acquire a negative charge of -22.7 ± 3.6 mV when mixed with DNA or RNA due to the negative charge of the nucleic acids.¹⁹ In this scenario, liposome formulations exhibited a ζ -potential of -25 mV. The hybridization process increased the surface charge of Hybs from about -21 mV (for EMNVs) to a maximum of ~ -11 mV (for the highest amounts of liposomes used for Hyb formulation) (Figure 1F).

To comprehensively investigate the efficiency of liposome-EMNV fusion during hybrid fabrication, we conducted fluorescence resonance energy transfer (FRET) analysis utilizing the DiO-DiI FRET pair. HEK293T cells were stained with the DiO lipophilic dye and subsequently extruded to obtain DiO-labeled EMNVs. Concurrently, RNA and Lipofectamine 3000 reagent were employed for liposome production, followed by the incorporation of the DiI lipophilic dye into the liposomes. To compare the efficiency of the fusion process, DiO-labeled EMNVs and DiI-labeled liposomes were utilized for hybrid production under four conditions: (1) simple mixing; (2) mixing followed by incubation at 37°C for 15 min; (3) incubation at 37°C for 15 min followed by extrusion; and (4) overnight incubation at 4°C.²⁰ FRET analysis demonstrated a notably higher efficiency of the extrusion process in generating Hybs (Figures S2 and 1G).

To conclude, these results indicate that our protocol has superior efficiency for synthesizing Hybs from EMNVs within the desired size range of ~130 nm.

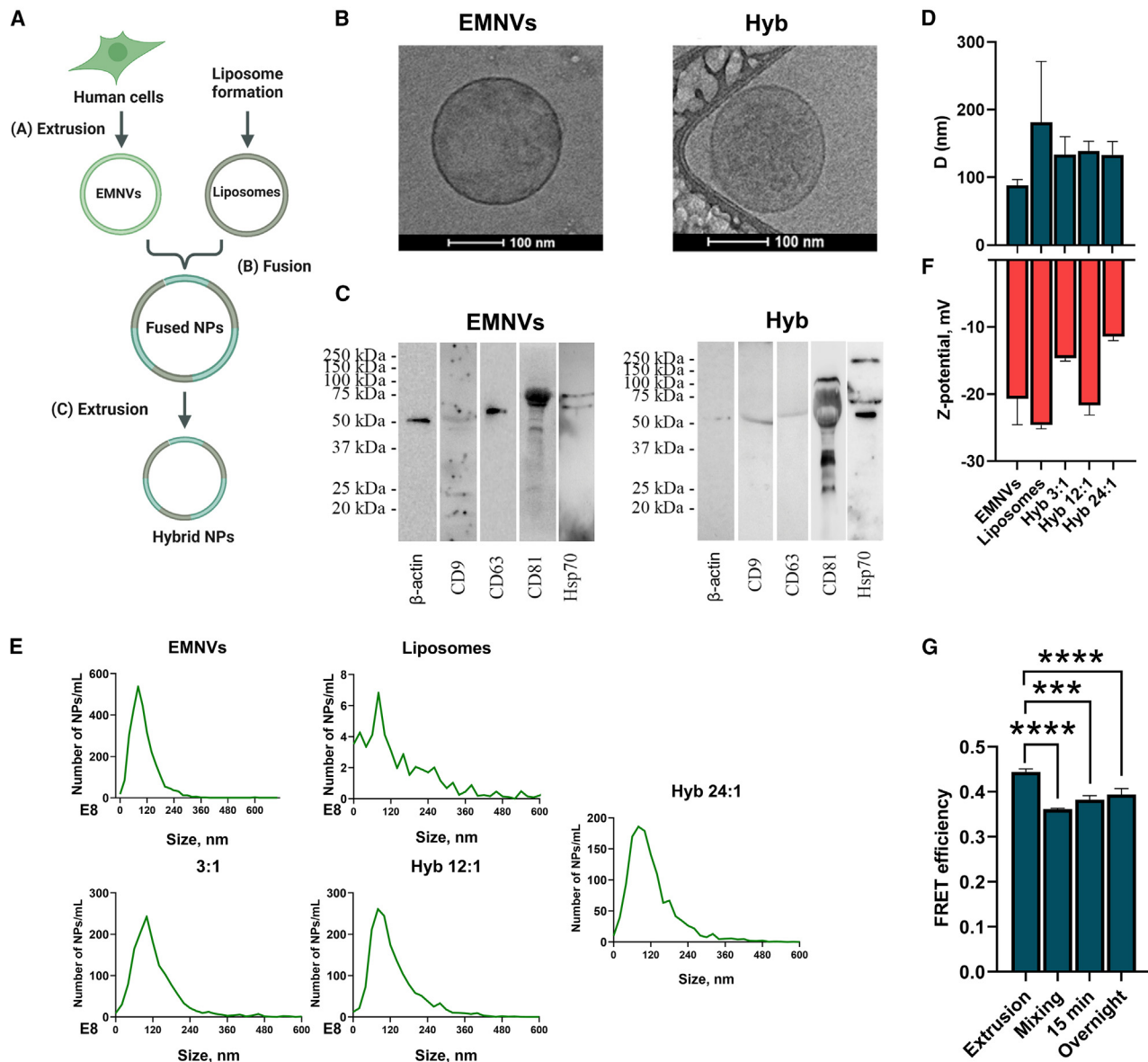


Figure 1. Fabrication and characterization of Hybs

(A) Technological schematic of Hyb synthesis process. (B) Cryo-TEM images of EMNVs and Hybs. (C) Western blot analysis of protein markers in EMNVs and Hybs. (D) Mean size, (E) ζ -potential, and (F) size distribution of different formulations of Hyb: fractions indicate liposome/EMNVs ratios. (G) FRET efficiency for fusion of EMNVs with liposomes. Mixing, mixing of liposomes with EMNV; 15 min, incubation for 15 min at 37°C; extrusion, extrusion of EMNVs with liposomes; overnight, overnight incubation of EMNVs with liposomes at 4°C. Error bars represent standard deviations. *** $p < 0.001$, **** $p < 0.0001$.

RNA packaging and intracellular delivery by EMNVs

Different approaches for RNA delivery using bioinspired nanovesicles were reviewed previously.²¹ We hypothesized that extrusion could increase the fusion with liposomes and RNA packaging yield in Hybs compared to previous methods. Thus, we used the same protocol for synthesizing Hybs from EMNVs and liposomes loaded with RNA (Figure 2A). As expected, Hybs generated via extrusion showed a 2-fold increase in RNA loading capacity compared to frequently

used short-term and long-term incubation at different temperatures (Figures S2 and 2B). Using real-time qPCR and different initial doses of RNA and three different ratios of liposomes to EMNVs, we showed an RNA dose-dependent (Figure 2C) and liposome-dependent increase in packaging efficiency of Hybs (Figure 2D). Moreover, there was a constraint on the RNA loading capacity of the NPs. Increasing the RNA dose from 2× to 4× did yield a proportional increase in the amount of loaded RNA (Figure 2C). Our calculation demonstrates

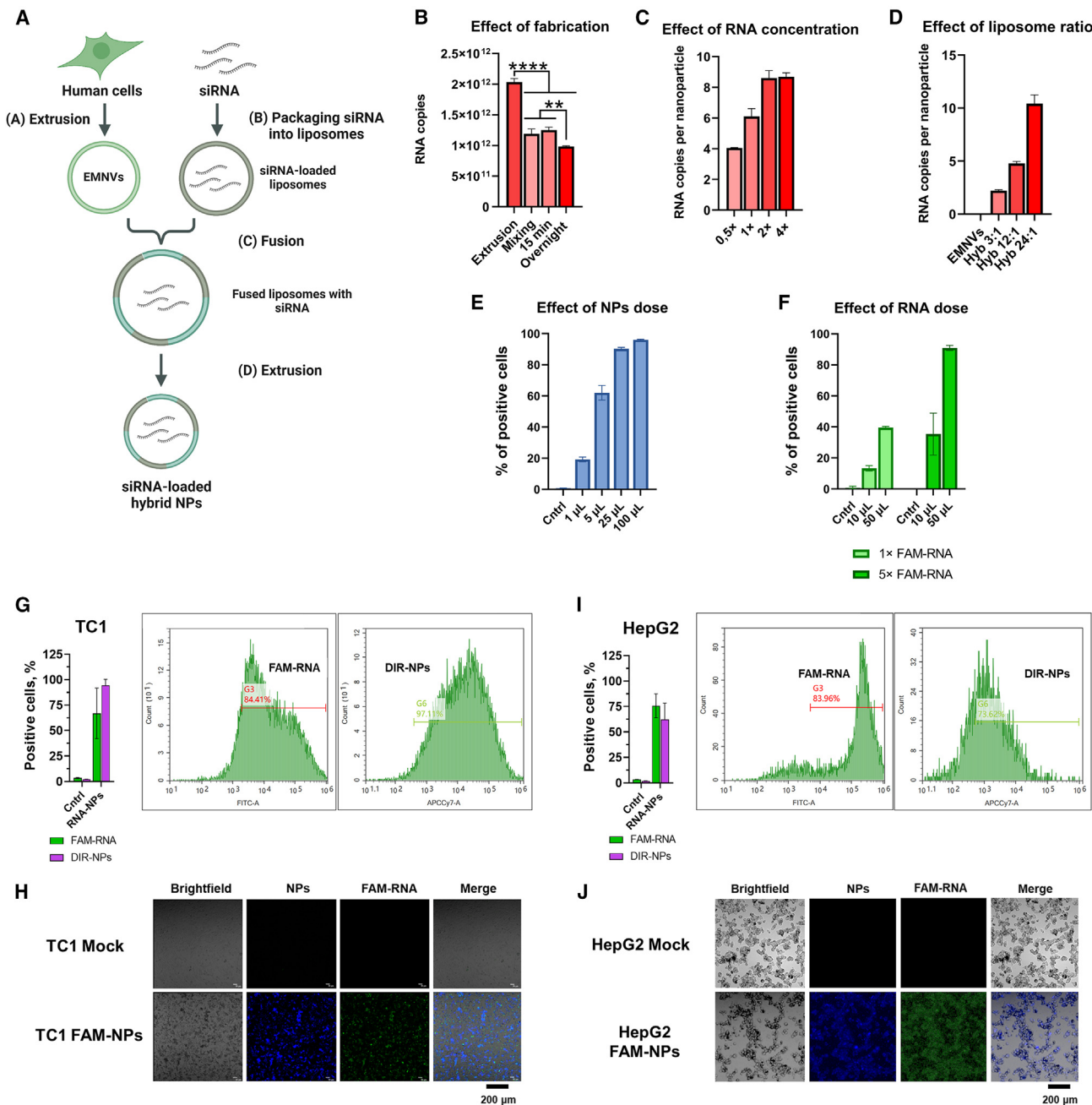


Figure 2. Packaging and intracellular delivery of RNA using Hybs

(A) Schematic of RNA loading into Hybs. (B) Effect of synthesis protocol on RNA loading efficiency. (C) Effect of RNA concentration on loading efficiency of Hybs (EMNVs/liposomes ratio 1:3). (D) Effect of Hyb formulation on RNA loading efficiency (EMNVs/liposomes ratio: 3:1, 12:1, and 24:1). (E) Hyb-dose-dependent and (F) FAM-RNA-concentration-dependent increase in HepG2 internalization measured by flow cytometry at APCcy7 (for DIR-labeled NPs) and FITC channels, respectively. (G) Internalization of FAM-RNA-loaded hybrid NPs into mouse TC1 cells and (H) representative fluorescent images. (I) Internalization of FAM-RNA-loaded Hybs into HepG2 cells and (J) representative fluorescent images. Fluorescent DIR-labeled Hybs (blue); FAM-RNA (green). Error bars represent standard deviations. ***p* < 0.01, *****p* < 0.0001.

that using 1:1 ratio of EMNVs/liposomes with 31.2 μg of RNA for 2.227×10^{13} NPs resulted in an average of 10.4 copies of RNA per Hyb (Figure 2D).

To test the ability of Hybs to deliver RNA intracellularly, FAM (FAM-11-dUTP, a fluorescein deoxyuridine triphosphate)-labeled RNA (FAM-RNA) was packaged into Hybs produced from a lipophilic

near-infrared fluorescent dye (DiR)-loaded EMNVs and FAM-RNA-loaded liposomes. Increasing concentrations of DiR-labeled hybrid NPs led to enhanced uptake by HepG2 cells, reaching ~96% (Figures 2E and S3). Similarly, experiments investigating the effect of varying FAM-RNA loading on Hybs demonstrated a concentration-dependent increase in FAM-positive cells. Utilizing $1 \times$ FAM-RNA resulted in a maximum of about 40% FAM-positive cells, while using $5 \times$ FAM-RNA led to a significant increase, reaching up to 91% FAM-positive cells (Figures 2F and S4).

Treating hard-to-transfect mouse TC1 cells (Figures 2D, 2E, and S5) or human HepG2 cells (Figures 2F, 2G, and S6) with Hybs demonstrated internalization of NPs and delivery of FAM-RNA into ~84% of cells. At the same time, we observed an increase in the percentage of fluorescent cells that depended on the dose of Hybs, reaching 100% when 2.5×10^9 NPs were used in 0.16×10^6 cells (Figures S3 and S4). Further experiments with DiR-labeled and FAM-RNA-loaded Hybs proved high efficiency of NP uptake and FAM-RNA delivery into both mouse cells (Figures 2G and 2H) and human cells (Figures 2I and 2J).

Together, these results demonstrate high and tunable packaging efficiency of our newly developed method and its ability to deliver RNA into ~91%–96% of cells.

Genetic functionalization of nanoparticles

Recently, efficient genetic functionalization platforms were applied to engineer the surface of exosomes and other EVs by modifying constitutive proteins with targeting molecules.^{12,22–26} Here, we used CD63 with truncated transmembrane domain 4 (Δ CD63),¹³ which is a convenient platform for exposing peptides on the surface of nanovesicles, and full-length PTGFRN¹⁴ for functionalizing EMNVs with liver-targeting apolipoprotein E (APOE) (Figure 3A). Moreover, we directly compared the efficiency of functionalizing EVs and EMNVs with the use of Δ CD63 and PTGFRN linked to EGFP. To this end, we produced EVs and EMNVs from HEK-293T cells transfected with Δ CD63-EGFP or EGFP-PTGFRN coding vectors. EVs were purified using size-exclusion chromatography and completely characterized (Figure S7). Equal amounts of carriers were used to directly compare EGFP fluorescence, which showed that PTGFRN was significantly more efficient at functionalizing EVs (Figure 3B), consistent with the initial study by Dooley et al.¹⁴ At the same time, functionalization of EMNVs was markedly more efficient than functionalization of EVs regardless of the platform used (Figure 3B).

Based on these results, we used EMNVs to compare targeting efficiencies of Δ CD63 and PTGFRN platforms with liver-targeting APOE in HepG2 cells, and toward this goal internalization studies were performed in flow conditions. EMNVs were labeled with lipophilic fluorescein isothiocyanate (FITC). As controls, we used untreated cells and cells treated with labeled but non-functionalized EMNVs. Flow-cytometry analysis demonstrated markedly improved internalization of PTGFRN-functionalized EMNVs (~84.6%) compared to Δ CD63 (~14.7%) (Figures 3C and 3D). Next, we inves-

tigated whether targeting properties of APOE-PTGFRN persisted in Hybs synthesized with the extrusion step. To do so, we produced EMNVs, APOE-functionalized EMNVs, Hybs, and APOE-functionalized Hybs and loaded them with Cy7 dye. The results confirmed higher internalization of APOE-functionalized EMNVs and demonstrated more efficient uptake of Hybs vs. EMNVs (~57.9% vs. ~42.6%), as well as significantly more efficient internalization of APOE-functionalized Hybs vs. Hybs (~68.7% vs. ~60.9%) (Figures 3E, 3F, and S8).

This study is the first to utilize two advanced functionalization platforms (PTGFRN and Δ CD63) to create targeted delivery vehicles using EMNVs and Hyb technology. These platforms achieved significantly higher functionalization efficiency compared to traditional methods using natural EVs. Furthermore, our findings demonstrated that full-length PTGFRN surpasses truncated CD63 in its ability to be efficiently incorporated into these delivery vehicles. This advantage of full-length PTGFRN is maintained even after hybridization with liposomes.

Interactions of EMNVs and Hybs with endolysosomal compartment

The major intracellular barrier for nanotherapeutics is entrapment in the endolysosomal compartment following degradation of the payload by hydrolytic enzymes in highly acidic pH.²⁷ Endolysosomal entrapment depends on the nature of the nanotherapeutic (size, charge, shape), internalization route, and its ability to escape these intracellular vesicles (e.g., via fusogenic, pH-sensitive peptides, “proton sponge” mechanisms, or direct fusion with the endosomal membrane).²⁸

To directly address the issue of RNA delivery, we investigated the behavior of EMNVs alone and RNA-loaded Hybs under physiologic (pH 7.4) and acidic conditions corresponding to early endosomes (pH 6.2), late endosomes (pH 5.5), and lysosomes (pH 4.5) for 15 min or 1 h (Figure 4A). The mean size of EMNVs slightly increased in acidic pH, indicating swelling, while EMNVs incubation at pH 4.5 for 1 h reduced the number of NPs. At the same time, the effect of acidic pH on Hybs was much more pronounced, since the particle reduction occurred during the first hour of incubation at pH 6.2 and further decreased at pH 5.5 and pH 4.5 (Figure 4A). Cryo-TEM imaging confirmed swelling and rupture of EMNVs and, more significantly, of Hybs (Figure 4B). To test the potential release of FAM-RNA from Hybs in acidic conditions, we incubated FAM-RNA-loaded Hybs at pH 4.5 or pH 7.4 for 15 min or 60 min and ran them on a gel to analyze electrophoretic mobility (Figure 4C). Particle integrity was assessed using gel electrophoresis. Intact particles can retain FAM-RNA inside, preventing its migration through the gel and resulting in no fluorescent signal. Conversely, if particle structure is compromised, FAM-RNA is released and can migrate during electrophoresis, generating a fluorescent band on the resolving gel. Indeed, incubating Hybs at pH 7.4 resulted in intense fluorescence at the high molecular weights of the gel, indicating that FAM-RNA was predominantly trapped inside Hybs (Figure 4D).

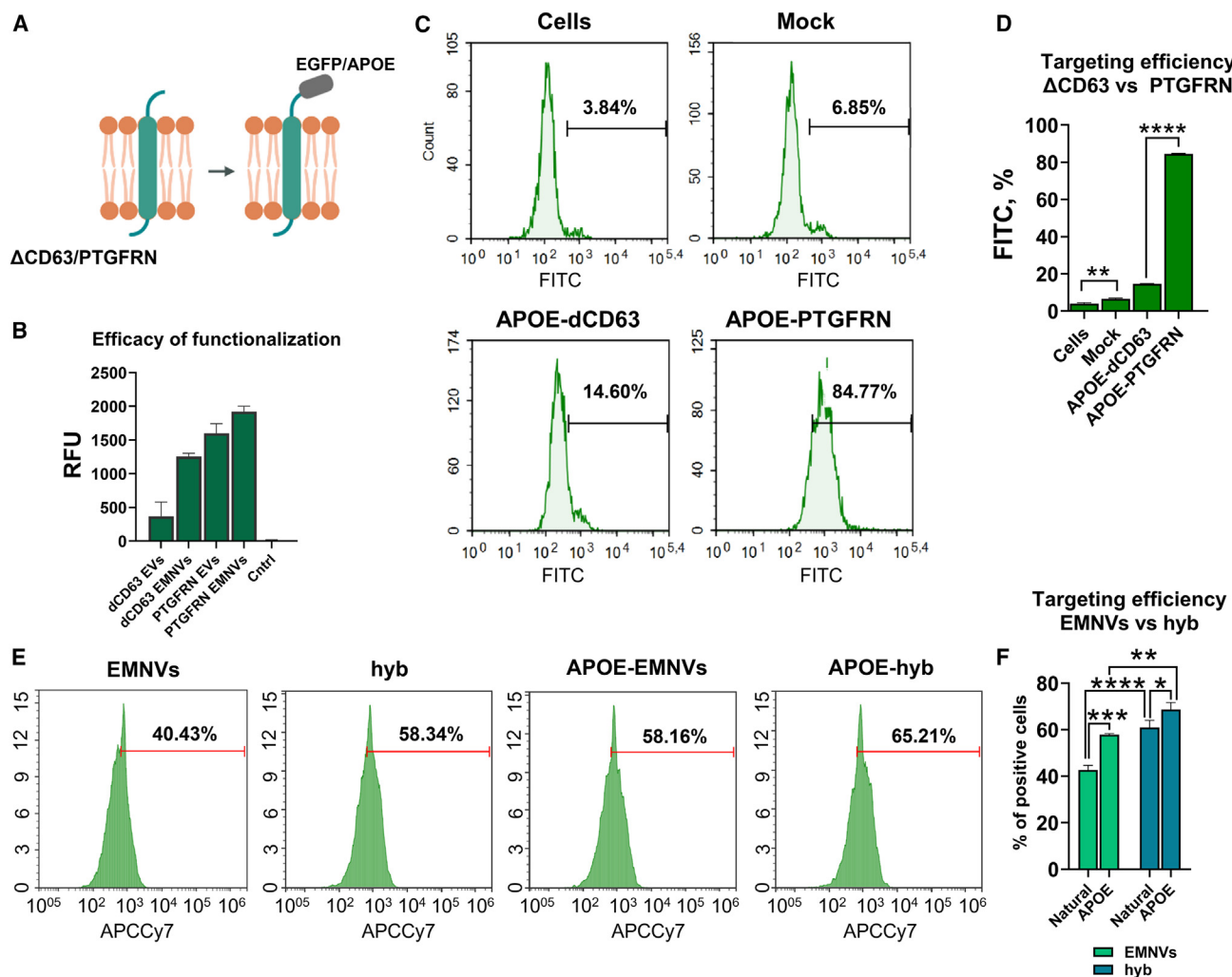


Figure 3. Functionalization of EVs, EMNVs, and Hybs

(A) Schematics of NP functionalization. (B) Comparison of Δ CD63 and PTGFRN genetic functionalization platforms for EVs and EMNVs using flow cytometry for assessing NP internalization by HepG2 cells in flow conditions. (C and D) Comparison of Δ CD63 and PTGFRN functionalization of EMNVs with APOE at HepG2 cells in flow conditions. (E and F) Comparison of APOE-PTGFRN functionalization for EMNVs and fabricated Hybs. Error bars represent standard deviations. * $p < 0.05$, ** $p < 0.01$, *** $p < 0.001$, **** $p < 0.0001$.

Contrastingly, acidic pH disrupted the integrity of Hybs, causing disappearance of the FAM fluorescent signal at high molecular weights (Figure 4D); under these conditions, FAM-RNA was detectable in all samples, potentially indicating leakage of FAM-RNA from NPs. Further analysis (Figures 4E and 4F) demonstrated stronger colocalization of Hybs with lysosomes compared to EMNVs (~50% for Hybs vs. ~30% for EMNVs). Testing different doses of hybrid NPs revealed statistically significant escape of low-dose Hybs over the course of the experiment (the first hour post treatment vs. 12–16 h post treatment). To investigate the role of lysosomes in the intracellular stability of EMNVs and Hybs, we loaded FAM-RNA into DiR-labeled EMNVs via electroporation or into Hybs fused with liposomes. These NPs were then applied to HepG2 cells treated with PBS or DMSO as control vehicles, or with potent, irreversible inhibitors of

cathepsins—namely E64 and PLVE—which are the most abundant lysosomal proteases.²⁹ Time-dependent inhibition of cathepsins by E64 or PLVE-FMK was shown at HepG2 cells with a fluorescent substrate Ac-QLLR-AMC (Figure S9). Time-lapse dynamic imaging of DiR-labeled and FAM-RNA-loaded NPs revealed a significant increase in the signal from Hyb NPs with any of the cathepsin inhibitors and no effect on the signal from EMNVs (Figures 4G and S10). A similar effect was not observed with FAM-RNA in any of the NPs used, possibly because the cleaved FAM-RNA molecules retain their fluorescence (Figure 4H). Together, these data indicate that (1) fusion of EMNVs with liposomes increases entrapment of NPs with endolysosomal compartment (Figures 4E and 4F) and (2) lysosomal proteases attenuate activity of Hybs, but not EMNVs (Figures 4G and 4H). In conclusion, the observed behavior indicates the entrapment of

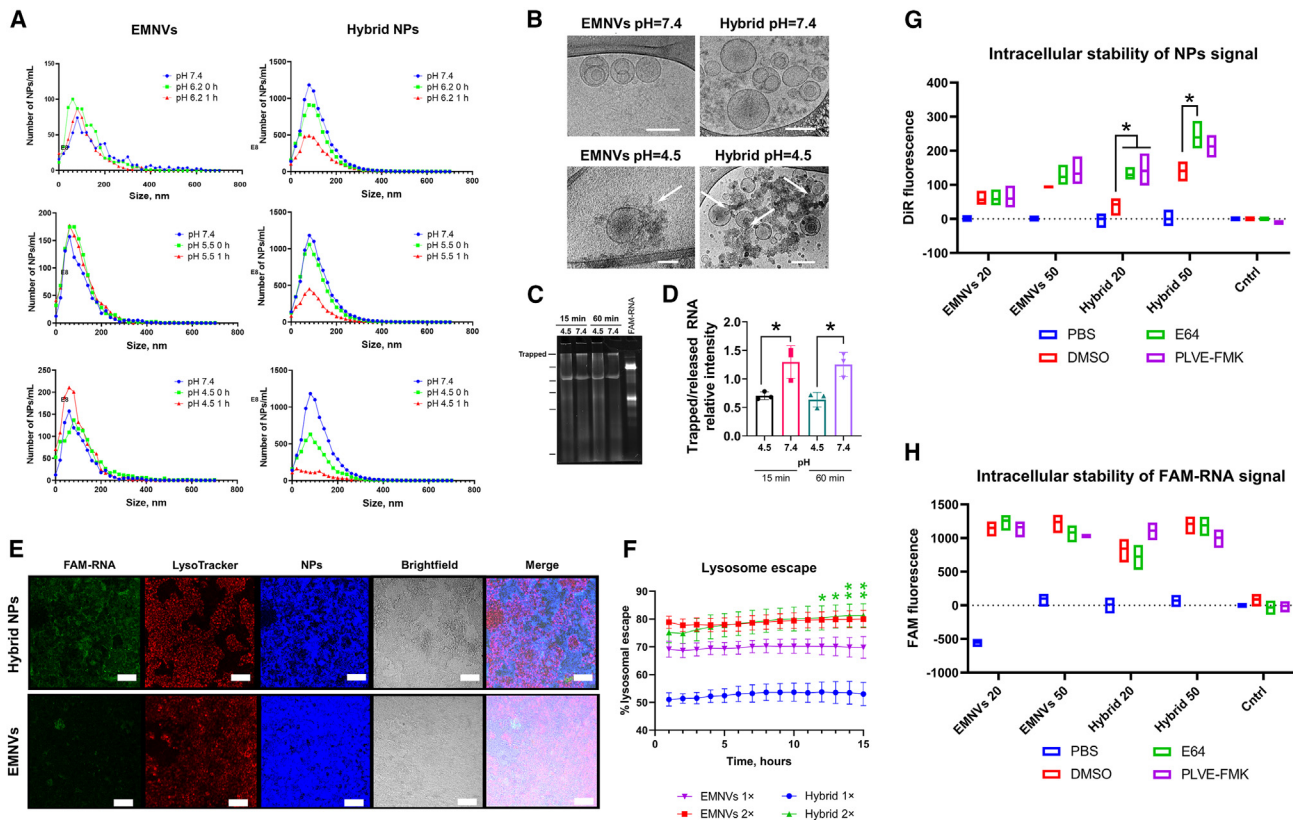


Figure 4. Effects of acidic pH on the properties of Hybs

(A) Changes in size and quantity of EMNVs and Hybs in acidic pH conditions. (B) Cryo-TEM images demonstrating swelling and rupture of EMNVs and Hybs. (C) Release of FAM-RNA from hybrid NPs upon short-term and 1-h incubation at pH 4.6. (D) Semi-quantitative analysis of released FAM-RNA. (E) Representative images of LysoTracker (red) with FAM-RNA (green) delivered by Hybs or EMNVs over time. Blue, HepG2 cells that internalized DiR-labeled NPs. Scale bar, 90 μ m. (F) Kinetics of FAM-RNA colocalization with lysosomes and escape of two doses of Hybs or EMNVs. Intracellular stability of (G) DiR-labeled NPs and (H) FAM-RNA delivered by Hybs or EMNVs. The values represent the mean signal for two concentrations of EMNVs or Hybs, which were treated with either PBS or cathepsin inhibitors (E64 or PLVE-FMK) over a time period of 4–44 h following the addition of NPs. Cntrl, HepG2 cells not treated with NPs. Differences were assessed using one-way or two-way ANOVA, where applicable. Error bars represent standard deviations. * $p < 0.05$, ** $p < 0.01$, *** $p < 0.001$, **** $p < 0.0001$; ns, non-significant difference.

Hybs within the endolysosomal compartment, which reduces their stability. Over time, Hybs escape this compartment, whereas EMNVs preferentially avoid it.

Hybrid nanoparticles potentially reduce HBV transcription and replication

Chronic hepatitis B (CHB), caused by hepatitis B virus (HBV) infection, is one of the world's most widespread diseases, with mortality rates exceeding 1 million people annually. One promising medication for suppressing HBV is based on transcriptionally silencing it using siRNA. For targeted delivery of siRNA, we produced non-functionalized and APOE-functionalized Hybs from PTGFRN-APOE-expressing HEK-293T cells and siRNA-loaded liposomes (Lipo), as shown in Figure 5A.

To test the applicability of Hybs for delivering therapeutic cargo, we used previously described siRNA targeting the X gene of HBV (Figure 5B). We then compared the efficacy and toxicity of these NPs in HepG2 cells with HBV replication driven from recombinant cova-

lently closed circular DNA (cccDNA), a well-established model of HBV replication,^{30–33} as shown in Figure 5C. As a result, all NPs reduced HBV biomarkers, including X-mRNA/pregenomic RNA (pgRNA) and pgRNA expression, intracellular HBV DNA, HBxAg, and HBsAg, whereas cccDNA was, as expected, not reduced by siRNA (Figures 5D–5I). HBsAg was reduced by all NPs, but this reduction was not statistically significant (Figure 4J). APOE-functionalized Hybs were on par with non-functionalized NPs, whereas the liposomal formulation was generally more effective but very toxic, as evidenced by reduced actin expression (Figure 5H), annexin V analysis (Figure 5K), and MTT (3-(4,5-dimethylthiazol-2-yl)-2,5-diphenyltetrazolium bromide) assay (Figure 5L). In total, Hybs exhibit prominent efficiency and are safe for cells.

Functionalized nanoparticles demonstrate the highest anti-HBV activity in vivo

Next, Cy7-labeled Hybs with and without APOE functionalization were injected into the tail vein of BALB/C mice to investigate their

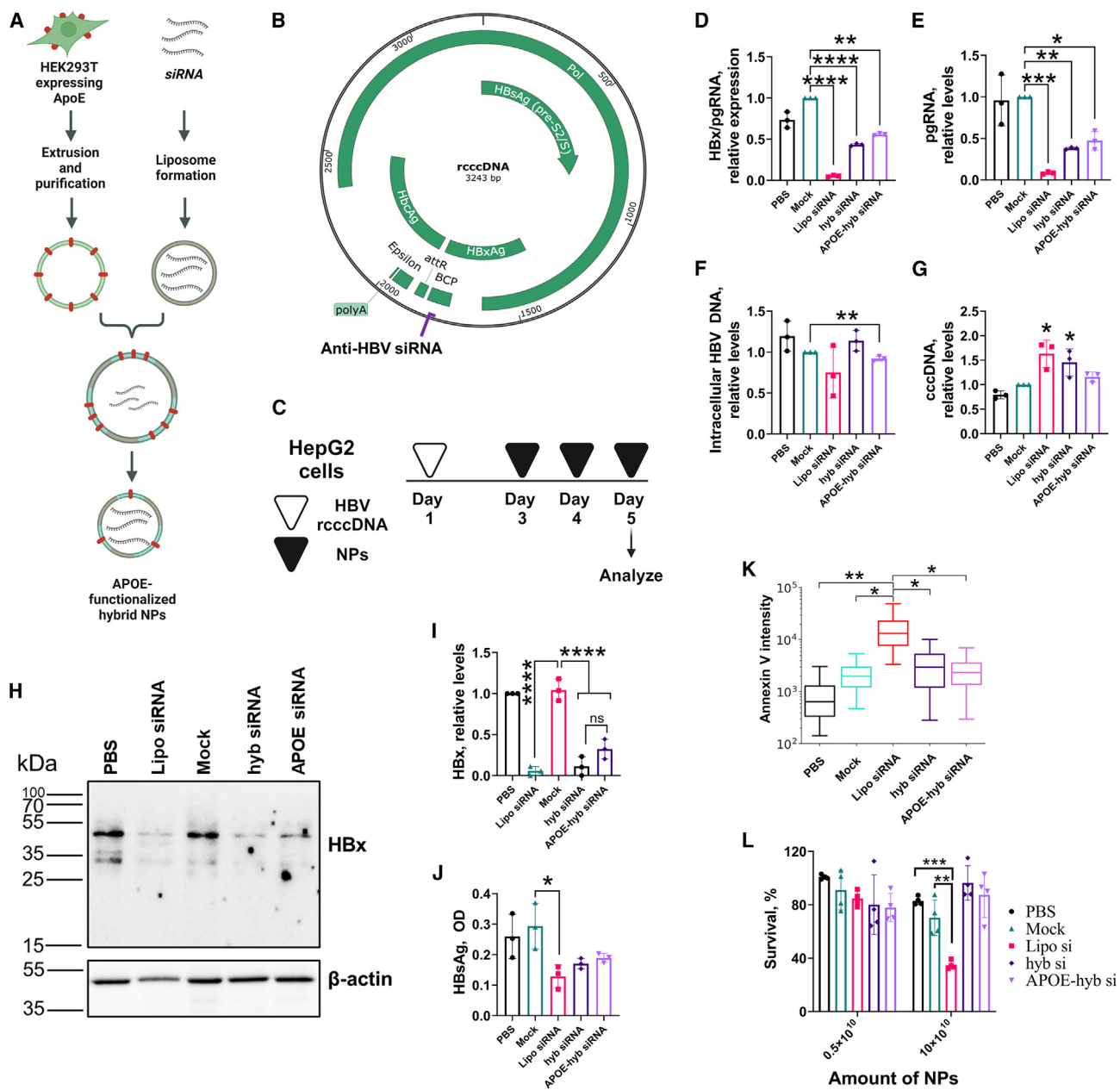


Figure 5. Antiviral activity of NPs loaded with siRNA in an HBV *in vitro* model

(A) Schematics for producing functionalized siRNA-loaded Hybs. (B) siRNA target in the HBV genome. (C) Experimental pipeline. Antiviral activity assessed by measuring (D) HBx/pgRNA, (E) pgRNA, (F) intracellular HBV DNA, and (G) cccDNA, and by (H) western blot analysis of HBxAg and (I) corresponding HBxAg level and (J) HBsAg level analysis. (K) Apoptosis analysis measured by annexin V expression and (L) MTT analysis of NP cytotoxicity. PBS, treatment of rcccDNA-transfected cells with PBS; Mock, treatment with EMNV NPs loaded with non-targeting siRNA. Error bars represent standard deviations. * $p < 0.05$, ** $p < 0.01$, *** $p < 0.001$, **** $p < 0.0001$.

biodistribution 1 h post injection. Expectedly, both the carriers preferentially accumulated in the liver, but APOE functionalization significantly increased liver targeting >2-fold (Figures 6A, 6B, and S11). Histological analysis of mice livers revealed uniform distribution of DiR-labeled NPs throughout the organ's parenchyma, similar for both Hybs and APOE-Hybs (Figure 6C).

To test therapeutic activity, BALB/C mice were injected with rcccDNA, and 3 days thereafter received equal daily doses of 0.3 mg/kg siRNA-loaded carriers (Figure 3D), the minimal effective concentration used previously.³⁴ On day 8 after the start of the experiment the mice were sacrificed, and serum and livers were harvested for further analysis. Analysis of HBsAg and HBV DNA in the serum

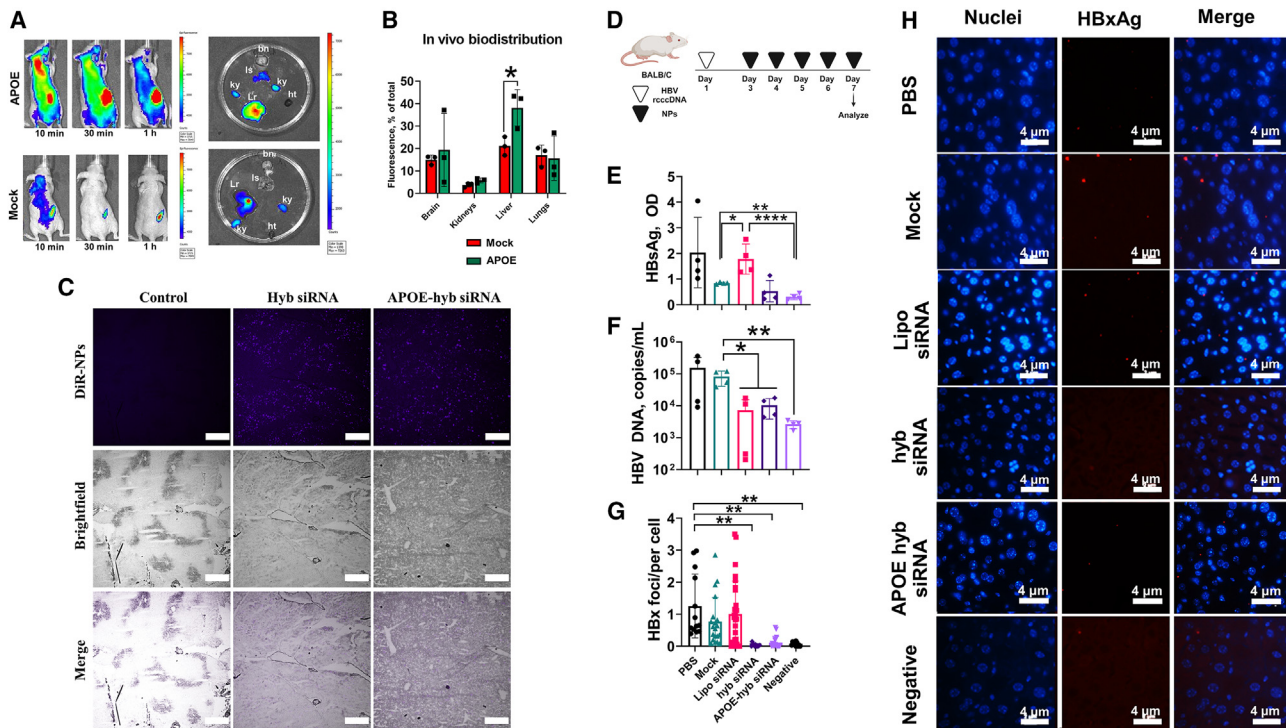


Figure 6. In vivo targeting and antiviral activity of siRNA-loaded Hybs

(A) Biodistribution of non-functionalized (Mock) and targeted (APOE) Hybs in mice and explanted organs. Bn, brain; ls, lungs; ky, kidneys; ht, heart; Lr, liver. (B) Semi-quantitative analysis of NP biodistribution. (C) Histological analysis of DiR-labeled NP biodistribution in liver cryosections. (D) Experimental design for assessing anti-HBV activity *in vivo*. (E) HBsAg. (F) HBV DNA. (G) Quantitative immunohistological analysis of HBxAg in liver sections. (H) Representative images of liver sections with counter-stained nuclei (blue) and HBxAg (red). PBS, treatment of rcccDNA-injected mice with PBS; Mock, treatment with EMNV NPs loaded with non-targeting siRNA; negative – mice that did not receive rcccDNA, and were injected with PBS. Error bars represent standard deviations. * $p < 0.05$, ** $p < 0.01$, *** $p < 0.001$, **** $p < 0.0001$.

revealed significant anti-HBV activity of APOE-functionalized Hybs (~64% reduction of HBsAg and >1.5 log reduction of HBV DNA) (Figures 6E–6G). A similar but less pronounced decline in HBV biomarkers was observed with siRNA-loaded Hybs. Liposomal siRNA formulation did not affect HBsAg levels but significantly reduced HBV DNA by 1 log. The primary target of siRNA, X-mRNA, which encodes HBxAg, was markedly reduced by both functionalized and non-functionalized Hybs with no apparent differences between the groups, as evidenced by immunohistological analysis. Liposomal siRNA was not effective.

To conclude, Hybs showed high potential in delivering RNA molecules, while their genetic functionalization with targeting peptides significantly improved the targeting and therapeutic efficacy of nanoformulations in an *in vivo* HBV model.

DISCUSSION

The emergence of RNA therapeutics—including RNA interference molecules, mRNA vaccines, and RNA-encoded gene modifiers such as CRISPR-Cas nucleases, base editors, and CRISPR activators/repressors—has significantly expanded the toolbox for tackling previously untreatable diseases. However, this progress necessitates the

development of advanced, targeted delivery systems to effectively utilize these technologies. Currently, various LNP formulations, polymers, and dendrimers are employed successfully to deliver RNA therapeutics. The field is actively exploring even more sophisticated delivery vehicles, such as virus-like particles, inorganic NPs (e.g., gold, graphene, silica), DNA-based nanostructures (e.g., DNA origami, nanoshells, nanoclews), and biological NPs. Among these, biological and bioinspired NPs have garnered significant interest due to their natural origin, high safety profile, and ability to overcome biological barriers for efficient cellular delivery.^{7,35–37} EMNVs, membrane NPs such as nanoghosts, and biomimetics have appeared as next-generation biological NPs with apparent advantages over EVs in terms of scalability, homogeneity, and manufacturing. In particular, manufacturing EMNV is 10–1,000-fold more efficient than manufacturing EVs, with EMNVs showing similar biodistribution, delivery efficiency, and active and passive tropism.^{7,38}

An important step in loading RNA into EVs was taken by Piffoux et al., who performed polyethylene glycol (PEG)-mediated fusion of liposomes with EVs to create biosynthetic hybrid vectors for RNA delivery.¹⁶ Later, similar strategies were implemented in dozens of studies using lipid film hydration and extrusion,³⁹ simple fusion,^{26,40}

and fusion with siRNA loading by electroporation.⁴¹ Extrusion has become a useful method to produce biomimetic NPs by fusing cell membranes or EVs with other types of particles, such as gold carriers and liposomes.⁴²

Previous studies have established initial approaches for fabricating hybrid liposomes-exosomes and have demonstrated the feasibility of delivering RNA and DNA cargo using these hybrids.^{16,26,39,40} In particular, Liang et al.²⁶ developed a treatment strategy for osteoarthritis based on chondrocyte-targeting exosomes that display a chondrocyte-affinity peptide via a Lamp2b genetic functionalization platform. These exosomes were fused with liposomes produced from Lipofectamine 3000 and CRISPR-Cas9-expressing plasmids targeting the MMP13 enzyme. Fusion was achieved through simple mixing of the two components, as evidenced by FRET assays and an increase in NP size detected by NP-tracking analysis (NTA). The injection of the produced hybrid NPs into the knee joint effectively alleviated osteoarthritis in a rat model *in vivo*.²⁶ In this study, we developed a novel pipeline for fabricating Hybs from EMNVs or, in fact, any type of biological NPs, with targeted properties and loaded with any RNA molecules. One of the most common protocols for producing hybrids with liposomes and biological NPs involves simple incubation at 37°C or prolonged incubation at 4°C.⁴³ Fusion between liposomes and biological NPs is induced by electrostatic interactions between cationic liposomes and negatively charged biological NPs, as well as by hydrophobic interactions. FRET assays using DiO-labeled EMNVs and DiI-labeled exosomes demonstrated a low efficiency of the simple incubation process compared to our protocol (Figure 1F). Additionally, prolonged overnight incubation resulted in a significant loss of labile RNA molecules during the hybridization process (Figure 2B). The application of an extrusion process following short-term incubation markedly increased the hybridization efficiency (Figure 1F) and enhanced the packaging of RNA into hybrid vesicles (Figure 2B).

Altering the amounts of EMNVs/liposomes ratio and RNA concentration enables tunable loading of cargo into synthesized nanocarriers (Figures 2C–2F). This protocol offers several important advantages for biomedical applications. First, the use of EMNVs instead of commonly used EVs significantly increases the yield of hybrid vesicles and the homogeneity of the final products, given that EV products are often poorly standardizable and costly. Second, the extrusion process results in controllable sizes of the final vesicles, which is favorable for pharmacokinetics and standardization purposes. Third, this protocol is based on the use of commercially available Lipofectamine reagent, making it accessible for hybrid production in almost any laboratory without requiring the establishment of a complicated liposome workflow or the use of expensive lipid reagents. Methods developed in this study do not use immunogenic or cytotoxic substances, such as PEG⁴⁴ or polyethylenimine,⁴⁵ nor use harsh conditions compromising stability and activity of RNA molecules or components of biological NPs such as freeze-thaw, acidic pH, or electroporation.^{16,39,41,46} Moreover, the developed technologies are straightforward and easily scalable, providing the means for large-scale manufacturing of stand-

ardizable NPs and overcoming the principal drawbacks of EVs and other NP formulations of non-biological origin.^{7,9}

Investigating physicochemical properties of Hybs revealed previously unknown behavior important for understanding the mechanism of payload delivery and endolysosomal escape. Acidification results in swelling and cracking of hybrid NPs much more efficiently than of EMNVs, resulting in effective release of RNA payload and escape of hybrid NPs from the endolysosomal compartment over time. Importantly, such behavior is observed at even slightly acidic conditions (pH 6.2), corresponding to early endosome conditions, and progressively exacerbates upon further acidification to pH 4.5, observed in lysosomes. This behavior may be beneficial in terms of endolysosomal escape, resulting in their rupture and subsequent release of NPs and their cargo. Moreover, time-lapse colocalization analysis revealed that Hybs were initially trapped in the endolysosomal compartment but escaped over time, while EMNVs predominantly avoided this compartment. This hypothesis was further supported by experiments assessing NP stability, which demonstrated that lysosomal cathepsin inhibitors did not affect the signal from EMNVs but significantly increased the signal from Hybs. These findings indicate that the fusion of EMNVs with liposomes alters their intracellular trafficking, rendering them more susceptible to lysosomal degradation (Figure 4). While the mechanisms of NP endolysosomal escape are complex and frequently rely on many routes,²⁷ we demonstrate a natural ability of hybrid NPs to effectively deliver RNA payload into target cells, achieving efficient gene knockdown (Figure 5).

Our generated Hybs were able to be internalized up to 96% in hard-to-transfect cell lines and to deliver RNA into >91% of mouse and human cells. Efficiency of RNA delivery directly depended on the amount of loaded RNA and the dose of NPs used during the treatment. Using two of the most advanced functionalization platforms for EVs, we demonstrated their superior applicability for functionalizing EMNVs and identified PTGFRN as the more efficient genetic platform over Δ CD63. To the best of our knowledge, this is the first indication that such technologies are useful and even more efficient for functionalizing biological NPs other than EVs. Importantly, functionalization persisted even after hybridization of EMNVs with liposomes. The use of PTGFRN for programming the surface of EMNVs and Hybs by APOE peptide demonstrated significant increase in internalization of functionalized NPs into hepatoma cells *in vitro* and into mouse liver *in vivo*. When loaded with anti-HBV siRNA, these functionalized NPs exhibited prominent antiviral activity and significantly higher anti-HBV potency *in vivo*. Although the use of liposomes does not fully reflect the potential advantages of biological NPs or Hybs,⁴⁷ it was still important to analyze the effect of liposomes, EMNVs, and Hybs on cell viability. MTT assay and apoptosis analyses using annexin V staining revealed high toxicity of the liposome-siRNA formulation compared to EMNVs or siRNA-loaded Hybs, consistent with previous observations that fusing liposomes with biological NPs increases liposome safety (Figures 5K and 5L).

In this work we provided a ready-to-use, scalable pipeline for producing Hybs for a broad range of practical applications, with targeted delivery of Hybs based on targeting peptides, toward advancing the field of biologics-based treatments.

MATERIALS AND METHODS

Cell cultures and transfection

Human cell lines HEK-293T, HepG2, and mouse cell line TC1 were cultured in complete medium, consisting of 4.5 g/L DMEM (PanEco, Moscow, Russia) supplemented with 10% fetal bovine serum (FBS) (HyClone, Cytiva), 2 mM L-glutamine (PanEco), 100 U/mL penicillin, and 100 µg/mL streptomycin (PanEco) at 37°C and 5% CO₂. HEK-293T cells were transfected using polyethyleneimine in NaCl, as described previously.^{6,32} In brief, HEK293-T cells were seeded in T225 225-cm² flasks at ~60% confluency the day before transfection. The next day, cells were transfected with a mix of solution A containing plasmid DNA (plasmid for functionalization) and solution B with polyethyleneimine in NaCl; the mixture was allowed to rest for 10 min before being added to cells. For cloning APOE- or EGFP-functionalization plasmids, plasmid PTGFRN (HsCD00867164) was purchased from DNASU Plasmid Repository (USA), and truncated CD63 developed from CD63-pEGFP C2 was a gift from Paul Luzio (Addgene plasmid #62964; <http://n2t.net/addgene:62964>; RRID: Addgene_62964). EGFP plasmid was cloned from plasmid CD63-pEGFP C2. The day after transfection, cells were washed with PBS (PanEco) and cultured in complete medium for the next 2 days. On the day of harvest, cells were washed in PBS and detached from culture plates using Versene solution (PanEco).

HepG2 cells were seeded at 70% confluency in 6-well plates the day before transfection, then transfected with rcccDNA using Lipofectamine 3000 (Thermo Fisher Scientific, USA), as described previously.^{30,33,48,49} In brief, 200 mg of rcccDNA (genotype D; HBV-encoding plasmid was kindly provided by Dieter Glebe, University of Giessen) in fectoMEM (Bioinnlabs, Russia) with p3000 reagent was mixed with Lipofectamine reagent in fectoMEM, incubated for 10 min, and added directly to HepG2 cells. Two days after transfection, cells were washed with PBS and cultured in complete DMEM medium with EV-depleted FBS. EV depletion was achieved by ultrafiltration of FBS through Amicon Ultra-4 100 kDa (Merck Millipore, USA), as described previously.⁵⁰

Fabrication of EMNVs

HEK-293T cells (~2 × 10⁷ cells per fabrication), resuspended in PBS, were extruded using a mini-extruder (Avanti Polar Lipids, USA) at 37°C with a set of hydrophilic polycarbonate track membranes (GVS, Italy) soaked in PBS-HAT (PBS supplemented with human albumin and trehalose) solution.⁵¹ The membranes had the following diameters: 10 µm (9 extrusions), 5 µm (9 extrusions), and 1 µm (9 extrusions). The resulting suspension was centrifuged at 4°C, 2,000 × g, for 5 min to remove cell debris. The supernatant was extruded 15 times through a polycarbonate membrane with pore diameter of 0.1 µm at 37°C. Biological NPs were purified using size-exclusion

chromatography on a 1.6 × 10-cm column with Sepharose CL-4B crosslinked agarose (Cytiva), with PBS as the mobile phase. Forty fractions with a final volume of 500 µL were collected. Fractions 11–16, containing biological NPs, were pooled and concentrated, if necessary, using Amicon Ultra-4 (10 kDa cutoff; Merck Millipore). Isolates of biological NPs were mixed in 10× storage PBS-HAT buffer⁵¹ for 1× concentration. For DiR staining of EMNVs and hybrid NPs, detached cells were mixed with DMEM supplemented with 5 µM LumiTrace DiR (Lumiprobe, Russia), and incubated with agitation (37°C, 350 × rpm) for 30 min followed by washing with PBS and subsequent extrusion process.

Fabrication of hybrid NPs

Suspensions of HEK-293T cells (~2 × 10⁷ cells per fabrication) were extruded as described for EMNVs. The suspensions derived after cell debris removal and a mix of 15.6 µg of *in vitro*-transcribed RNA (FAM-RNA or anti-HBV siRNA) and 20 µL of Lipofectamine 3000 reagent (Thermo Fisher Scientific, USA), incubated for 10 min in advance, were incubated for 20 min at 37°C for fusion. For analyzing RNA loading into hybrid NPs using real-time qPCR and gel-electrophoresis analysis of FAM-RNA, artificial RNA of 160 bp was synthesized. After fusion, the suspension was extruded 15 times through a polycarbonate membrane with 0.1-µm pores at 37°C. The resultant hybrid NPs were isolated and stored as described for EMNVs.

Isolation of EVs

EVs were isolated from conditioned medium of HEK-293T cells cultured in complete DMEM with EV-depleted FBS for at least 2 days.^{6,7} In brief, conditioned medium was serially centrifuged at 2,000 × g for 10 min and then at 10,000 × g for 10 min to remove cell debris and microvesicles before being applied to columns with MacroPrep DEAE medium anion-exchange resin (Bio-Rad, Hercules, CA, USA) to isolate EVs by anion-exchange chromatography, as shown by Heath et al.⁵² The column was washed consecutively with 100% buffer A (50 mM HEPES, 100 mM NaCl), 95% buffer A/5% buffer B (50 mM HEPES, 2 M NaCl; 5 column volumes), and 90% buffer A/10% buffer B (10 column volumes). Fractions with EVs were first eluted in 60% buffer A/40% buffer B and then concentrated using Amicon Ultra-15 (100 kDa) filter devices.

Fluorescent labeling of NPs

Biological NPs (~5 × 10¹¹) were mixed with near-infrared dye Sulfo-Cyanine7 carboxylic acid (Lumiprobe, Russia) at a concentration of 500 µg/mL and exposed to two freeze-thaw cycles. After the second thaw, the resulting suspension was extruded through a 0.1-µm hydrophilic polycarbonate track membrane (GVS, Italy) using a mini-extruder (Avanti Polar Lipids; 11 repetitions). Free dye was removed by washing the suspension three times in PBS using a VivaSpin 500 protein concentrator (300 kDa cutoff; Sartorius, Germany). Alternatively, NPs were labeled with DiR lipophilic dye (Lumiprobe, Russia), FITC-fluorescent dye ExoGlow-Membrane EV Labeling Kit (Green) (SBI, USA) or DiO lipophilic dye (Lumiprobe, Russia).

FRET analysis

Twenty million cells were detached from T225 (225 cm²) flasks by Versene solution (PanEco, Russia) and resuspended in a medium containing 2.5 μM DiO, incubated at 37°C with agitation, and centrifuged at 350 rpm for 45 min. The medium was discarded, and the cells were washed three times with PBS solution. Next, cells were used for the extrusion process for producing EMNVs. Extrusion was performed using 10-μm, 5-μm, and 1-μm filters (seven times). Cellular debris was removed by centrifugation at 2,000 × *g* for 5 min, and the supernatant was divided into four equal parts. In parallel, 15.6 μg of RNA was mixed with 100 μL of OptiMEM and incubated at room temperature for 10 min. DiI dye (1 μM) was then added before incubation for another 10 min at 37°C. Produced liposomes were divided into four equal parts, similarly to EMNV suspension. EMNV parts were mixed with liposomes. The first mix was purified by gel-filtration chromatography using the low-pressure chromatography system Bio-Lab 30 (Hanbon, China) immediately after mixing (Mixing); the second part was incubated for 15 min at 37°C and then purified (15 min); the third part was incubated for 15 min at 37°C, then extruded through a 0.1-μm filter (11 times) and purified (Extrusion); and the fourth part was incubated overnight at +4°C and then pooled. Fractions corresponding to particles were collected and pooled. Equal volumes of samples were measured using a ClarioStar plate fluorimeter at wavelengths of 420/535 (fluorescence of the donor, F_d) and 420/630 (fluorescence of the acceptor, F_a). FRET efficiency was calculated using the formula $E = F_a / (F_d + F_a)$.

Flow-cytometry analysis

Cells were analyzed on a LongCyte (Challengebio, China) flow cytometer using FITC and APCCy7 channels. Data analysis was performed using ModelFlower software.

Confocal and high-content fluorescent microscopy

HepG2 cells were treated with LysoTracker. Hybrid NPs loaded with FAM-RNA were added to HepG2 cells prestained with LysoTracker. The fluorescence intensity and distribution of the LysoTracker Red DND-99 (Thermo Fisher Scientific) dye were analyzed using an Olympus FV3000 microscope; kinetic analysis was performed using and LCI Image ExFluor Microscope (Live Cell Instrument, South Korea). Colocalization analysis was performed in Image ExFluor Software. Mander colocalization coefficients were calculated in ImageJ using the JACoP plugin.

Assessment of NP functionalization

NP functionalization efficiency was assessed by measuring EGFP fluorescence exhibited on the surface of NPs. HEK-293T cells were transfected with ΔCD63-EGFP or PTGFRN-EGFP plasmids using polyethylenimine as described above. Three days thereafter, the cells were used for producing EMNVs and isolating EVs. Equal numbers of NPs measured by NTA were collected for analysis. Next, fluorescence in corresponding samples was measured using a ClarioStar Plus plate fluorimeter (excitation/emission = 470/515 nm). Efficacy of functionalization was compared as relative fluorescence units of membrane-bound EGFP.

Production of rcccDNA

HBV rcccDNA, genotype D, was generated by minicircle technology, as described in previous studies.^{30,33} *E. coli* strain ZYCY10P3S2T (System Biosciences) containing the HBV genome (genotype D) cloned between attB and attP recombination sites was incubated in lysogeny broth (LB) with kanamycin at 37°C for 4 h, then inoculated into 200 mL of Terrific broth and incubated overnight at 37°C to 600 nm optical density of 6–8 and pH 7.0. Finally, recombination of attB and attP sites was induced by 200 mL of induction medium (1 N NaOH and 0.2% L-arabinose in LB) for 3 h at 30°C followed by incubation for 1 h at 37°C. HBV rcccDNA was isolated from the bacterial pellets using Plasmid Mediprep (Evrogen, Russia).

Western blotting

EVs were lysed as previously described⁶ using RIPA buffer (50 mM Tris-HCl [pH 8.0], 150 mM NaCl, 0.1% Triton X-100, 0.5% sodium deoxycholate, 0.1% SDS, 1 mM NaF) followed by sonication. Samples in 6× Laemmli buffer were loaded onto 10% SDS-PAGE and transferred onto nitrocellulose membranes. The membranes were blocked in 5% milk in TBS-T (20 mM Tris [pH 7.5], 150 mM NaCl, 0.1% Tween 20), then stained with primary antibodies EXOAB-KIT-1 (anti-CD63, anti-CD9, anti-CD81, anti-Hsp70; SBI, USA) and anti-β-actin antibodies (A1978, Sigma). Membranes were washed three times with TBS-T and incubated for 1 h with goat anti-rabbit HRP-conjugated antibodies (Ab6721; Abcam, Cambridge, MA, USA) or with goat anti-mouse HRP-conjugated antibodies (Ab6787; Abcam) followed by three washes in TBS-T. Chemiluminescent signal was developed using Clarity Max substrate SuperSignal West Femto Maximum (Bio-Rad, USA) and detected with Chemscope 6200 touch (X-ray filmsClinx, China). Alternatively, HepG2 cells were lysed in RIPA buffer and 6× Laemmli buffer and used for SDS-PAGE and immunostaining with primary anti-HBx antibodies (ab39716, Abcam) and anti-β-actin antibodies (A1978, Sigma).

Synthesis of siRNA

PCR product encoding siRNA under control of T7 promoter was synthesized using Q5 high-fidelity DNA polymerase (NEB) using overlap extension PCR with the following primers:

siHBV74_fw: AAg CTA ATA CgA CTC ACT ATA ggg ACC AAT TTA TgC CTA CAg CCT TCA AgA gAg gCT gT; siHBV74_rev: AgA CAT AAA AAA CAA AAA AAg ACC AAT TTA TgC CTA CAg CCT CTC TT. PCR product was resolved by agarose gel electrophoresis and purified by a DNA Cleanup Mini kit (Evrogen). Next, the PCR product was used as a template for *in vitro* transcription reaction using the In Vitro Transcription Kit (Biolabmix, Russia) by overnight incubation according to the manufacturer's instructions. The reaction mixture was then treated with DNase I (NEB) for 15 min at 37°C. RNA was purified by precipitation with isopropanol in NaCl and washed consecutively with 70% and 95% ethanol. The air-dried pellet was dissolved in RNase-free water and stored at –20°C before use. FAM-labeled RNA was produced using the same protocol with FAM-11-UTP (Lumiprobe, Russia) added to the

reaction mixture. Artificial RNA was synthesized as described previously with primers ultramerT7_f and ultramerSt1_r.^{30,49}

Annexin V analysis

The FITC-annexin V reagent (Lumiprobe, Russia) was used according to the manufacturer's protocol. Analysis of apoptosis was performed both on cells on the plate and on the floating cells in cell-culture medium. Cells on the plate were detached using trypsin-EDTA solution (PanEco, Russia). The mixture of detached and floating cells was washed twice with ice-cold PBS and resuspended in binding buffer at a final density of 10^6 cells/mL. Next, 2 μ L of FITC-annexin V reagent (0.02 mg/mL) and 5 μ L of ethidium bromide (EtBr) (0.1 mg/mL) were added to 100 μ L of the cell suspension containing 10^5 cells. Cell suspension was vortexed gently and incubated for 15 min at room temperature in darkness. Subsequently, cells were resuspended in 400 μ L of binding buffer and analyzed by flow cytometry (LongCyte, Challenbio).

MTT assay

To evaluate the impact of NPs on cell viability, HepG2 cells were seeded into 96-well plates at a density of 10×10^3 , and the following day treated with increasing concentrations of NPs. Four replicate wells were used for each condition and control. The treatment was performed overnight, after which the MTT assay was used to determine the effect of NPs on cell viability. The tetrazolium salt (MTT) was dissolved in PBS (5 mg/mL), added to HepG2 cells as described previously,^{53,54} and incubated for 3 h at 37°C. Thereafter, 1 N hydrogen chloride–isopropanol (1:24, v/v) was added and mixed to dissolve formed formazan crystals. Fluorimetric analysis was performed at 570 nm in a SuPerMax3100 microplate reader (Shanghai ShineGene, China).

Enzymatic kinetic study of cathepsin inhibition

Assessment of cathepsin inhibition by E64 and PLVE-FMK was performed as described earlier.⁵⁵ In brief, Ac-QLLR-AMC (MedChemExpress, USA), a substrate for lysosomal cathepsins, was added to HepG2 cells. Fluorescence resulting from cathepsin degradation of the substrate was analyzed dynamically using a SuPerMax3100 microplate reader (Shanghai ShineGene, China). 20 μ M PLVE-FMK and 50 μ M E64 were added to HepG2 cells for cathepsin inhibition, with PBS used as vehicle.

Electroporation-assisted loading of FAM-RNA into EMNVs

HEK-293T cells (2×10^7 cells per fabrication) were resuspended in PBS and extruded using a mini-extruder (Avanti Polar Lipids, USA) at 37°C, employing a set of hydrophilic polycarbonate track membranes (GVS, Italy) soaked in PBS-HAT solution.⁵¹ The membranes had the following diameters: 10 μ m (7 extrusions), 5 μ m (7 extrusions), and 1 μ m (7 extrusions). The resulting suspension was centrifuged at 4°C and $2,000 \times g$ for 5 min to remove cell debris. Subsequently, 30 μ g of FAM-RNA was added to the supernatant of the engineered microvesicles (EMNVs) and gently mixed. The mixture was transferred into an electroporator cuvette and pulsed using a Bio-Rad MicroPulser electroporator with a program specifically de-

signed for HEK293T cells. The solution was incubated at 37°C for 10 min and extruded 11 times through a polycarbonate membrane with a pore diameter of 0.1 μ m at 37°C. FAM-loaded EMNVs were purified using size-exclusion chromatography on a 1.6×10 -cm column containing Sepharose CL-4B crosslinked agarose (Cytiva), with PBS serving as the mobile phase. Isolates of FAM-labeled biological NPs were subsequently mixed with a $10\times$ storage PBS-HAT buffer to achieve a $1\times$ concentration.

Analysis of intracellular stability of NPs

Two doses of DiR-labeled and FAM-RNA-loaded EMNVs or Hybs (for $1\times$ and for $2\times$, respectively) were added to HepG2 cells. After 4 h, conditioned medium was discarded, and cells were washed twice in PBS and supplemented with complete medium. DiR and FAM-RNA fluorescent imaging was then performed using an LCI Ex-Fluor microscope (LCI, South Korea).

Isolation of nucleic acids from nanoparticles

RNA from hybrid NPs was isolated using a total ExtractRNA kit (Evrogen) and reverse transcribed using AmpliSens Reverta-FL (AmpliSens Biotechnologies, Russia) according to the manufacturer's protocol.

Isolation of nucleic acids from cells

Cells washed in PBS were lysed in lysis buffer (AmpliSens Biotechnologies), and nucleic acids were isolated using an AmpliSens Riboprep kit according to the manufacturer's protocol. For removing DNA, samples were treated with DNase I (NEB), purified by an AmpliSens Riboprep kit, and reverse transcribed by AmpliSens Reverta-FL. HBV cccDNA isolated via Hirt procedure was treated with T5 exonuclease (NEB) at 37°C for 60 min followed by inactivation at 70°C for 20 min.

PCR analysis

Real-time PCR was performed using DTprime 5M6 PCR amplifiers (DNA-Technologies, Russia) with SybrGreen dye (for HBx-mRNA) or TaqMan probes (for GAPDH mRNA, pgRNA, β -globin, HBV DNA, and cccDNA) with sets of primers described previously.^{56,57} Artificial RNA (aRNA) was detected using a set of the following primers and probes: aRNA_f AGA AAG GCC TTG TAA GTT GG; aRNA_r GCC ATA AAA TGA CAG GGT G; aRNA_probe ACA AAG ATA AGG CTT CAT GC. PCR results were analyzed using the $\Delta\Delta C_t$ method.

In vivo experiments

Female BALB/C mice, 5–7 weeks old, were obtained from the animal breeding facility of the N.N. Blokhin Russian Cancer Research Center. All animal experiments were performed in accordance with Russian law and were approved by the Ethics Committee of the Blokhin Cancer Research Center. Mice were injected into the tail vein with NPs in PBS-HAT at a final volume of 100 μ L (three mice per group). The control group received 100 μ L of non-functionalized NPs. Biodistribution was analyzed using IVIS Spectrum CT (PerkinElmer) on 745-nm and 800-nm excitation/emission wavelengths 10 min,

30 min, and 1 h post injection. Mice received inhaled isoflurane anesthesia during biodistribution analysis. At 1 h post injection, mice were anesthetized by inhaled isoflurane followed by cervical dislocation. Organs were explanted from sedated mice euthanized by cervical dislocation. Data are presented as the percentage of organ fluorescence from the total fluorescence of all organs as show in Wiklander et al.⁵⁸

***In vivo* HBV experiments**

Female BALB/C mice, 5–7 weeks old, were obtained from the animal breeding facility of the N.N. Blokhin Russian Cancer Research Center and transferred to Chumakov Federal Scientific Center for Research and Development of Immunobiological Products, Russian Academy of Sciences (Polio Institute) for HBV experiments in 2–3 BLS-licensed facilities. Animal experiments were performed in accordance with Russian law and were approved by the Ethics Committee of the Polio Institute. At day 1 of the experiment, mice received 380 ng of HBV rcccDNA (genotype D) per mice in 2 mL of PBS by hydrodynamic injection as described previously.⁵⁹ After injection, mice were placed on a heating pad and monitored for the next 1 h. At 3 days post injection, mice started receiving daily doses of 200 μ L of NPs in PBS (four mice per group). At day 7, mice were sacrificed by cervical dislocation, and blood was collected using cardiac puncture into EDTA-containing tubes. Serum was isolated by centrifugation for 10 min at 2,000 \times g and 4°C. Liver was explanted and fixed in 4% paraformaldehyde. 6- μ m-thick sections were used for immunohistochemistry (IHC) analysis.

Immunohistochemistry

IHC was performed according to the protocol described in Kostyusheva et al.⁵⁷ Cryosections were obtained from optimal-cutting-temperature blocks of mouse liver fixed in 4% paraformaldehyde solution for 10 min, washed three times for 10 min in 50 mM Tris-HCl (pH 8.0), incubated in blocking buffer (0.02% Triton X-100, 10% horse serum, 150 mM NaCl in 50 mM Tris-HCl [pH 8.0]) for 30 min, and incubated with primary rabbit polyclonal anti-HBxAg antibodies (ab39716; Abcam, UK) for 1 h at room temperature. After washing 3 \times 10 min with washing buffer (0.02% Triton X-100, 200 mM NaCl in 50 mM Tris-HCl [pH 8.0]), sections were incubated with secondary goat anti-rabbit antibodies Alexa Fluor 488 (ab15077, Abcam) and Hoechst33324 reagent (Abcam, ab228351) for 1 h at room temperature. The sections were then washed 3 \times 10 min in washing buffer and fixed with a Fluoroshield reagent (ab104135, Abcam). Fluorescent images were taken using an LCI ExFluor microscope (LCI, South Korea). The analysis of DiR-labeled NP biodistribution in cryosectioned liver was conducted without any treatments, as the DiR signal tends to fade upon fixation.

HBsAg analysis

Conditioned medium or mouse serum was used for quantifying HBsAg using a colorimetric ELISA-based test system, DS-IFA-HBsAg-0.01 (Diagnostic Systems), according to the manufacturer's instructions.

Nanoparticle-tracking analysis

Preparations of NPs were analyzed and quantified using an LM10 HS unit (NanoSight, Amesbury, UK) equipped with a 405-nm laser. Videos of NP tracking were recorded with passive temperature readout and the following parameters: camera shutter 1,500, camera gain 500, lower threshold 195, and higher threshold 1,885. Videos were analyzed using analytical software version 2.3 (NanoSight, Amesbury, UK) with a detection threshold of 8 multi.

ζ -Potential measurements

ζ -Potential of NPs was analyzed at least five times using a Zetasizer NanoZS instrument (Malvern, Worcestershire, UK) in U-type cuvettes (DTS1070; Malvern) with gold electrodes at 25°C. NP preparations were first diluted in PBS 1:1,000. The background signal was measured in filtered PBS.

Dynamic light scattering analysis

A Zetasizer NanoZS instrument (Malvern) was used for the dynamic light scattering analysis of all biological and hybrid biological NPs. Each NP preparation was diluted 1:1,000 in PBS with a corresponding pH and analyzed five times; 1.5 mL of diluted preparations were loaded into polystyrene cuvettes (DTS0012; Malvern). Analyses were performed at 25°C (100 measurements) using a 20-mW helium/neon laser (633 nm). Data were analyzed in Zetasizer software 8.01.4906 (Malvern). The background signal was measured in filtered PBS.

Native PAGE

20 μ L of hybrid EMNVs loaded with FAM-RNA were mixed with 1.62 μ L of 2 M NaOAc (pH 4.6) or with PBS (pH 7.4) and incubated for 15 min or 60 min at room temperature. Next, the samples were mixed with 4 \times sample loading buffer (125 mM Tris-HCl [pH 6.8], 20% glycerol [v/v], 0.004% bromophenol blue [w/v]). The samples were separated on a 14% native PAGE and analyzed using the Bio-Rad ChemiDoc MP Imaging system equipped with an Alexa 488 filter. The intensity of the FAM-RNA bands was determined using GelAnalyzer 19.1 software.

Cryo-TEM

NPs were pipetted onto a lacy carbon-supported copper grid (200 mesh) treated with air plasma. The excess of the sample was removed by blotting the grid for 1 s. The grid was plunged into liquid ethane (automated plunging system, Vitrobot FEL, USA). The grid was then transferred in liquid nitrogen to the transmission electron microscope (Tecnai G212 SPIRIT; FEI, USA).

Statistical analysis

Values were expressed as mean \pm SD. Student's t test or one-way ANOVA with Tukey's HSD post hoc test were used to compare variables and calculate *p* values to identify statistically significant differences in means. Time-lapse imaging experiments were calculated using ordinary two-way ANOVA.

DATA AND CODE AVAILABILITY

All data are available from the corresponding author upon reasonable request.

ACKNOWLEDGMENTS

This study was funded by Russian Science Foundation no. 20-15-00373-P. ζ -Potential measurements were supported by the Ministry of Science and Higher Education of Russia, no. 075-01551-23-00 (FSSF-484 2023-0006) (V.S.P.). NTA characterization was supported by Academic Leadership Program Priority 2030 (Sechenov University).

AUTHOR CONTRIBUTIONS

A.K. and S.B. were responsible for the study concept, design, and, together with N.P., for conducting all the experiments, analysis, data interpretation, and drafting and revisions of the manuscript. A.L., E.B., G.B., I.K., D. Sokolova, I.G., and V.S.P. conducted and analyzed *in vivo* experiments. O.S., P.D., G.M., D. Silachev, E.K., and A.A.Z. characterized all types of NPs. A.K. and A.T. assisted in fabrication and characterization of NPs, conducting *in vitro* experiments, and PCR analysis. V.C. and D.K. acquired funding, were responsible for the study design, concept, and supervision, and drafted and revised the manuscript.

DECLARATION OF INTERESTS

The authors declare no competing interests.

SUPPLEMENTAL INFORMATION

Supplemental information can be found online at <https://doi.org/10.1016/j.ymthe.2024.11.004>.

REFERENCES

1. El Andaloussi, S., Lakkal, S., Mäger, I., and Wood, M.J.A. (2013). Exosomes for targeted siRNA delivery across biological barriers. *Adv. Drug Deliv. Rev.* 65, 391–397.
2. Parodi, A., Quattrocchi, N., van de Ven, A.L., Chiappini, C., Evangelopoulos, M., Martinez, J.O., Brown, B.S., Khaled, S.Z., Yazdi, I.K., Enzo, M.V., et al. (2013). Synthetic nanoparticles functionalized with biomimetic leukocyte membranes possess cell-like functions. *Nat. Nanotechnol.* 8, 61–68.
3. Molinaro, R., Corbo, C., Martinez, J.O., Taraballi, F., Evangelopoulos, M., Minardi, S., Yazdi, I.K., Zhao, P., De Rosa, E., Sherman, M.B., et al. (2016). Biomimetic proteolipid vesicles for targeting inflamed tissues. *Nat. Mater.* 15, 1037–1046.
4. Oieni, J., Loll, A., D'Atri, D., Kops, N., Yayon, A., van Osch, G.J.V.M., and Machluf, M. (2021). Nano-ghosts: Novel biomimetic nano-vesicles for the delivery of antisense oligonucleotides. *J. Control Release* 333, 28–40.
5. Go, G., Lee, J., Choi, D.S., Kim, S.S., and Ghoo, Y.S. (2019). Extracellular Vesicle-Mimetic Ghost Nanovesicles for Delivering Anti-Inflammatory Drugs to Mitigate Gram-Negative Bacterial Outer Membrane Vesicle-Induced Systemic Inflammatory Response Syndrome. *Adv. Healthc. Mater.* 8, 1801082.
6. Brezgin, S., Kostyusheva, A., Ponomareva, N., Bayurova, E., Kondrashova, A., Frolova, A., Slatinskaya, O., Fatkhutdinova, L., Maksimov, G., Zyuzin, M., et al. (2023). Hydroxychloroquine Enhances Cytotoxic Properties of Extracellular Vesicles and Extracellular Vesicle – Mimetic Nanovesicles Loaded with Chemotherapeutics. *Pharmaceutics* 15, 534.
7. Brezgin, S., Parodi, A., Kostyusheva, A., Ponomareva, N., Lukashev, A., Sokolova, D., Pokrovsky, V.S., Slatinskaya, O., Maksimov, G., Zamyatnin, A.A., et al. (2023). Technological aspects of manufacturing and analytical control of biological nanoparticles. *Biotechnol. Adv.* 64, 108122.
8. Wang, F., Zuroske, T., and Watts, J.K. (2020). RNA therapeutics on the rise. *Nat. Rev. Drug Discov.* 19, 441–442.
9. Kostyushev, D., Kostyusheva, A., Brezgin, S., Smirnov, V., Volchkova, E., Lukashev, A., and Chulanov, V. (2020). Gene Editing by Extracellular Vesicles. *Int. J. Mol. Sci.* 21, 7362.
10. Brezgin, S., Kostyusheva, A., Kostyushev, D., and Chulanov, V. (2019). Dead Cas Systems: Types, Principles, and Applications. *Int. J. Mol. Sci.* 20, 6041.
11. Paunovska, K., Loughrey, D., and Dahlman, J.E. (2022). Drug delivery systems for RNA therapeutics. *Nat. Rev. Genet.* 23, 265–280.
12. Salunkhe, S., Basak, M., Basak, M., Chitkara, D., and Mittal, A. (2020). Surface functionalization of exosomes for target-specific delivery and *in vivo* imaging & tracking: Strategies and significance. *J. Control Release* 326, 599–614.
13. Curley, N., Levy, D., Do, M.A., Brown, A., Stickney, Z., Marriott, G., and Lu, B. (2020). Sequential deletion of CD63 identifies topologically distinct scaffolds for surface engineering of exosomes in living human cells. *Nanoscale* 12, 12014–12026.
14. Dooley, K., McConnell, R.E., Xu, K., Lewis, N.D., Haupt, S., Younis, M.R., Martin, S., Sia, C.L., McCoy, C., Moniz, R.J., et al. (2021). A versatile platform for generating engineered extracellular vesicles with defined therapeutic properties. *Mol. Ther.* 29, 1729–1743.
15. Nakase, I., and Futaki, S. (2015). Combined treatment with a pH-sensitive fusogenic peptide and cationic lipids achieves enhanced cytosolic delivery of exosomes. *Sci. Rep.* 5, 10112.
16. Piffoux, M., Silva, A.K.A., Wilhelm, C., Gazeau, F., and Tareste, D. (2018). Modification of Extracellular Vesicles by Fusion with Liposomes for the Design of Personalized Biogenic Drug Delivery Systems. *ACS Nano* 12, 6830–6842.
17. Welsh, J.A., Goberdhan, D.C.I., O'Driscoll, L., Buzas, E.I., Blenkiron, C., Bussolati, B., Cai, H., Di Vizio, D., Driedonks, T.A.P., Erdbrügger, U., et al. (2024). Minimal information for studies of extracellular vesicles (MISEV2023): From basic to advanced approaches. *J. Extracell. Vesicles* 13, e12404.
18. Xu, M., Qi, Y., Liu, G., Song, Y., Jiang, X., and Du, B. (2023). Size-dependent *in vivo* transport of nanoparticles: implications for delivery, targeting, and clearance. *ACS Nano* 17, 20825–20849.
19. Son, K.K., Patel, D.H., Tkach, D., and Park, A. (2000). Cationic liposome and plasmid DNA complexes formed in serum-free medium under optimum transfection conditions are negatively charged. *Biochim. Biophys. Acta* 1466, 11–15.
20. Lin, Y., Wu, J., Gu, W., Huang, Y., Tong, Z., Huang, L., and Tan, J. (2018). Exosome-Liposome Hybrid Nanoparticles Deliver CRISPR/Cas9 System in MSCs. *Adv. Sci.* 5, 1700611.
21. Xu, X., Xu, L., Wang, J., Wen, C., Xia, J., Zhang, Y., and Liang, Y. (2024). Bioinspired cellular membrane-derived vesicles for mRNA delivery. *Theranostics* 14, 3246–3266.
22. Liu, Q., Li, D., Pan, X., and Liang, Y. (2023). Targeted therapy using engineered extracellular vesicles: principles and strategies for membrane modification. *J. Nanobiotechnology* 21, 334.
23. Liang, Y., Duan, L., Lu, J., and Xia, J. (2021). Engineering exosomes for targeted drug delivery. *Theranostics* 11, 3183–3195.
24. Xu, L., Xu, X., Liang, Y., Wen, C., Ouyang, K., Huang, J., Xiao, Y., Deng, X., Xia, J., and Duan, L. (2023). Osteoclast-targeted delivery of anti-miRNA oligonucleotides by red blood cell extracellular vesicles. *J. Control Release* 358, 259–272.
25. Liang, Y., Xu, X., Li, X., Xiong, J., Li, B., Duan, L., Wang, D., and Xia, J. (2020). Chondrocyte-targeted microRNA delivery by engineered exosomes toward a cell-free osteoarthritis therapy. *ACS Appl. Mater. Inter.* 12, 36938–36947.
26. Liang, Y., Xu, X., Xu, L., Iqbal, Z., Ouyang, K., Zhang, H., Wen, C., Duan, L., and Xia, J. (2022). Chondrocyte-specific genomic editing enabled by hybrid exosomes for osteoarthritis treatment. *Theranostics* 12, 4866–4878.
27. Chatterjee, S., Kon, E., Sharma, P., and Peer, D. (2024). Endosomal escape: A bottleneck for LNP-mediated therapeutics. *Proc. Natl. Acad. Sci.* 121, e2307800120.
28. Qiu, C., Xia, F., Zhang, J., Shi, Q., Meng, Y., Wang, C., Pang, H., Gu, L., Xu, C., Guo, Q., and Wang, J. (2023). Advanced Strategies for Overcoming Endosomal/Lysosomal Barrier in Nanodrug Delivery. *Research (Wash D C)* 6, 0148.
29. Soond, S.M., Kozhevnikova, M.V., Townsend, P.A., and Zamyatnin, A.A., Jr. (2019). Cysteine Cathepsin Protease Inhibition: An update on its Diagnostic, Prognostic and Therapeutic Potential in Cancer. *Pharmaceutics* 12, 87.
30. Kostyushev, D., Kostyusheva, A., Brezgin, S., Ponomareva, N., Zakirova, N.F., Egorshina, A., Yanvarev, D.V., Bayurova, E., Sudina, A., Goptar, I., et al. (2023). Depleting hepatitis B virus relaxed circular DNA is necessary for resolution of infection by CRISPR-Cas9. *Mol. Ther. Acids* 31, 482–493.
31. Kostyushev, D., Brezgin, S., Kostyusheva, A., Zarifyan, D., Goptar, I., and Chulanov, V. (2019). Orthologous CRISPR/Cas9 systems for specific and efficient degradation of covalently closed circular DNA of hepatitis B virus. *Cell. Mol. LIFE Sci.* 76, 1779–1794.
32. Kostyusheva, A., Brezgin, S., Bayurova, E., Gordeyuk, I., Isaguliantis, M., Goptar, I., Urusov, F., Nikiforova, A., Volchkova, E., Kostyushev, D., et al. (2019). ATM and ATR Expression Potentiates HBV Replication and Contributes to Reactivation of HBV Infection upon DNA Damage. *Viruses* 11, 997.

33. Kostyushev, D., Brezgin, S., Kostyusheva, A., Ponomareva, N., Bayurova, E., Zakirova, N., Kondrashova, A., Goptar, I., Nikiforova, A., Sudina, A., et al. (2023). Transient and tunable CRISPRa regulation of APOBEC/AID genes for targeting hepatitis B virus. *Mol. Ther. Acids* 32, 478–493.
34. Gane, E., Lim, Y.S., Kim, J.B., Jadhav, V., Shen, L., Bakardjiev, A.I., Huang, S.A., Cathcart, A.L., Lempp, F.A., Janas, M.M., et al. (2023). Evaluation of RNAi therapeutics VIR-2218 and ALN-HBV for chronic hepatitis B: Results from randomized clinical trials. *J. Hepatol.* 79, 924–932.
35. Liang, Y., Iqbal, Z., Wang, J., Xu, L., Xu, X., Ouyang, K., Zhang, H., Lu, J., Duan, L., and Xia, J. (2022). Cell-derived extracellular vesicles for CRISPR/Cas9 delivery: engineering strategies for cargo packaging and loading. *Biomater. Sci.* 10, 4095–4106.
36. Duan, L., Ouyang, K., Wang, J., Xu, L., Xu, X., Wen, C., Xie, Y., Liang, Y., and Xia, J. (2021). Exosomes as targeted delivery platform of CRISPR/Cas9 for therapeutic genome editing. *Chembiochem.* 22, 3360–3368.
37. Iqbal, Z., Rehman, K., Xia, J., Shabbir, M., Zaman, M., Liang, Y., and Duan, L. (2023). Biomaterial-assisted targeted and controlled delivery of CRISPR/Cas9 for precise gene editing. *Biomater. Sci.* 11, 3762–3783.
38. Xu, X., Xu, L., Wen, C., Xia, J., Zhang, Y., and Liang, Y. (2023). Programming assembly of biomimetic exosomes: An emerging theranostic nanomedicine platform. *Mater. Today Bio* 22, 100760.
39. Evers, M.J.W., van de Wakker, S.L., de Groot, E.M., de Jong, O.G., Gitz-François, J.J.J., Seinen, C.S., Sluijter, J.P.G., Schifflers, R.M., and Vader, P. (2022). Functional siRNA Delivery by Extracellular Vesicle – Liposome Hybrid Nanoparticles. *Adv. Healthc. Mater.* 11, e2101202–e2101213.
40. Rayamajhi, S., Nguyen, T.D.T., Marasini, R., and Aryal, S. (2019). Macrophage-derived exosome-mimetic hybrid vesicles for tumor targeted drug delivery. *Acta Biomater.* 94, 482–494.
41. Jhan, Y.-Y., Prasca-Chamorro, D., Palou Zuniga, G., Moore, D.M., Arun Kumar, S., Gaharwar, A.K., and Bishop, C.J. (2020). Engineered extracellular vesicles with synthetic lipids via membrane fusion to establish efficient gene delivery. *Int. J. Pharm.* 573, 118802.
42. Parodi, A., Kostyushev, D., Brezgin, S., Kostyusheva, A., Borodina, T., Akasov, R., Frolova, A., Chulanov, V., and Zamyatnin, A.A., Jr. (2022). Biomimetic approaches for targeting tumor-promoting inflammation. *Semin. Cancer Biol.* 86, 555–567.
43. Liu, A., Yang, G., Liu, Y., and Liu, T. (2022). Research progress in membrane fusion-based hybrid exosomes for drug delivery systems. *Front. Bioeng. Biotechnol.* 10, 939441.
44. Chen, B.-M., Cheng, T.-L., and Roffler, S.R. (2021). Polyethylene glycol immunogenicity: theoretical, clinical, and practical aspects of anti-polyethylene glycol antibodies. *ACS Nano* 15, 14022–14048.
45. Lam, A.K., Moen, E.L., Pusavat, J., Wouters, C.L., Panlilio, H., Ferrell, M.J., Houck, M.B., Glatzhofer, D.T., and Rice, C.V. (2020). PEGylation of polyethylenimine lowers acute toxicity while retaining anti-biofilm and β -lactam potentiation properties against antibiotic-resistant pathogens. *ACS omega* 5, 26262–26270.
46. Cheng, L., Zhang, X., Tang, J., Lv, Q., and Liu, J. (2021). Gene-engineered exosomes-thermosensitive liposomes hybrid nanovesicles by the blockade of CD47 signal for combined photothermal therapy and cancer immunotherapy. *Biomaterials* 275, 120964.
47. Johnsen, K.B., Gudbergsson, J.M., Duroux, M., Moos, T., Andresen, T.L., and Simonsen, J.B. (2018). On the use of liposome controls in studies investigating the clinical potential of extracellular vesicle-based drug delivery systems - A commentary. *J. Control Release* 269, 10–14.
48. Kostyushev, D., Brezgin, S., Kostyusheva, A., Zarifyan, D., Goptar, I., and Chulanov, V. (2019). Orthologous CRISPR/Cas9 systems for specific and efficient degradation of covalently closed circular DNA of hepatitis B virus. *Cell. Mol. Life Sci.* 76, 1779–1794. <https://doi.org/10.1007/s00018-019-03021-8>.
49. Kostyushev, D., Kostyusheva, A., Brezgin, S., Zarifyan, D., Utkina, A., Goptar, I., and Chulanov, V. (2019). Suppressing the NHEJ pathway by DNA-PKcs inhibitor NU7026 prevents degradation of HBV cccDNA cleaved by CRISPR/Cas9. *Sci. Rep.* 9, 1847.
50. Kornilov, R., Puhka, M., Mannerström, B., Hiidenmaa, H., Peltoniemi, H., Siljander, P., Seppänen-Kajansinkko, R., and Kaur, S. (2018). Efficient ultrafiltration-based protocol to deplete extracellular vesicles from fetal bovine serum. *J. Extracell. Vesicles* 7, 1422674.
51. Görgens, A., Corso, G., Hagey, D.W., Jawad Wiklander, R., Gustafsson, M.O., Felldin, U., Lee, Y., Bostancioglu, R.B., Sork, H., Liang, X., et al. (2022). Identification of storage conditions stabilizing extracellular vesicles preparations. *J. Extracell. Vesicles* 11, e12238.
52. Heath, N., Grant, L., De Oliveira, T.M., Rowlinson, R., Osteikoetxea, X., Dekker, N., and Overman, R. (2018). Rapid isolation and enrichment of extracellular vesicle preparations using anion exchange chromatography. *Sci. Rep.* 8, 5730–5812.
53. Präßt, K., Engelhardt, H., Ringgeler, S., and Hübner, H. (2017). Basic Colorimetric Proliferation Assays: MTT, WST, and Resazurin. *Methods Mol. Biol.* 1601, 1–17.
54. Kolesova, E.P., Egorova, V.S., Syrocheva, A.O., Frolova, A.S., Kostyushev, D., Kostyusheva, A., Brezgin, S., Trushina, D.B., Fatkhutdinova, L., Zyuzin, M., et al. (2023). Proteolytic Resistance Determines Albumin Nanoparticle Drug Delivery Properties and Increases Cathepsin B, D, and G Expression. *Int. J. Mol. Sci.* 24, 10245.
55. Rudzińska, M., Parodi, A., Maslova, V.D., Efmov, Y.M., Gorokhovets, N.V., Makarov, V.A., Popkov, V.A., Golovin, A.V., Zernii, E.Y., and Zamyatnin, A.A., Jr. (2020). Cysteine Cathepsins Inhibition Affects Their Expression and Human Renal Cancer Cell Phenotype. *Cancers (Basel)* 12, 1310.
56. Kostyusheva, A.P., Kostyushev, D.S., Brezgin, S.A., Zarifyan, D.N., Volchkova, E.V., and Chulanov, V.P. (2019). Small Molecular Inhibitors of DNA Double Strand Break Repair Pathways Increase the ANTI-HBV Activity of CRISPR/Cas9. *Mol. Biol.* 53, 274–285.
57. Kostyusheva, A.P., Brezgin, S.A., Ponomareva, N.I., Goptar, I.A., Nikiforova, A.V., Gegechkori, V.I., Poluektova, V.B., Turkadze, K.A., Sudina, A.E., Chulanov, V.P., and Kostyushev, D.S. (2022). [Antiviral Activity of CRISPR/Cas9 Ribonucleoprotein Complexes on a Hepatitis B Virus Model In Vivo]. *Mol. Biol.* 56, 884–891.
58. Wiklander, O.P.B., Nordin, J.Z., O’Loughlin, A., Gustafsson, Y., Corso, G., Mäger, I., Vader, P., Lee, Y., Sork, H., Seow, Y., et al. (2015). Extracellular vesicle in vivo bio-distribution is determined by cell source, route of administration and targeting. *J. Extracell. Vesicles* 4, 26316.
59. Qi, Z., Li, G., Hu, H., Yang, C., Zhang, X., Leng, Q., Xie, Y., Yu, D., Zhang, X., Gao, Y., et al. (2014). Recombinant covalently closed circular hepatitis B virus DNA induces prolonged viral persistence in immunocompetent mice. *J. Virol.* 88, 8045–8056.